ELSEVIER

Journal of Nuclear Materials 254 (1998) 191–204

journal of nuclear materials

A molecular dynamics study of high-energy displacement cascades in α-zirconium

S.J. Wooding [*,1], L.M. Howe [2], F. Gao, A.F. Calder, D.J. Bacon

Department of Materials Science and Engineering, The University of Liverpool, Liverpool L69 3BX, UK

Received 23 July 1997; accepted 9 December 1997

Abstract

The damage produced in α-zirconium at 100 K by displacement cascades with energy, E_p, up to 20 keV has been investigated by molecular dynamics using a many-body interatomic potential. The results are compared with similar data for cascades of energy up to 10 keV in α-titanium. The production efficiency of Frenkel pairs falls to about 25% of the NRT value as E_p rises above 10 keV in zirconium, and to about 30% at 10 keV in titanium. The power-law dependence of the number of Frenkel pairs, N_F, on E_p found previously is obeyed, i.e., $N_F = A(E_p)^m$. Interstitial and vacancy clusters with sizes of the same order are created in the cascade process, and clusters containing up to 25 interstitials and 30 vacancies were formed in zirconium by 20 keV cascades. Two thirds of the SIAs are produced in clusters in zirconium at high cascade energy. Most interstitial clusters have dislocation character with perfect Burgers vectors of the form $1/3\langle 11\bar{2}0\rangle$, but a few metastable clusters are formed and are persistent over the timescale of MD simulations. Collapse of the 30-vacancy cluster to a faulted loop on the prism plane was found to occur over a period of more than 100 ps. Annealing over this timescale has a stronger effect on the number and clustering of defects in cascades that are dispersed over a large region of crystal than in cascades that form a compact region of damage. © 1998 Elsevier Science B.V.

1. Introduction

Computer simulation by molecular dynamics (MD) has proved to be a valuable technique for investigating the primary state of radiation damage during irradiation of metals by fluxes of fast atomic particles. It is able to provide information of not only the mechanisms that control the production of defects in displacement cascades but also the actual number and arrangement of the defects created. Such knowledge is crucial for the successful prediction and assessment of material performance in power-reactor systems.

As described in several recent reviews [1–4], there has been a rapid growth of activity in the modelling of cascades in the past few years, and this has increased understanding of the various collisional and thermal processes associated with cascade events. It has been concerned mainly with metals and alloys of the cubic crystal structures, although one study of α-titanium [5] and another on α-zirconium have been reported [6]. Alpha-zirconium is the more important HCP metal in this context because of its widespread use in fuel cladding, calandria tubes and pressure tubes in several current reactor systems [7,8]. The two previous studies [5,6] only considered cascades created by primary-recoil atoms (PKAs) with energy, E_p, up to 5 keV, however, whereas the average energy from a fission-neutron spectrum in a CANDU reactor, for example, is 19 keV ($E > 0.1$ MeV). It was therefore considered desirable to extend the MD simulations to higher PKA energy, and so we have now modelled defect production by cascades in zirconium with E_p up to 20 keV and, for purposes of

* Corresponding author.

[1] Present address: Unilever Research, Colworth House, Sharnbrook, Beds MK44 1LQ.

[2] Present address: AECL, Chalk River Laboratories, Chalk River, Ontario, Canada KOJ 1JO.

PII S0022-3115(97)00365-6

comparison, have simulated events in titanium for E_p up to 10 keV. In addition, it was found previously that many of the interstitial defects formed in cascades in these metals are mobile and so it was felt to be important to simulate the defects produced in some cascades for a longer time than that allowed in the low-energy studies.

The method employed is summarised in Section 2 and PKA energy effects on the ballistic phase of cascades are discussed in Section 3. Data for the final number of defects are presented in Section 4, and they are analysed in terms of the size distribution of defect clusters in Section 5. The crystallographic and geometrical features of some of the more interesting clusters are considered in Section 6. The effect of time on the defects during the first 100 ps after the cascade has finished and other aspects of the results are discussed in Section 7.

2. Model and method

The details of the interatomic potentials and computing method used here are to be found in the two earlier papers [5,6] and will not be repeated. The MD blocks were approximately cuboid in shape and had dimensions $56a_0 \times 32\sqrt{3}a_0 \times 35c_0$ for the 10 keV cascades and $72a_0 \times 41\sqrt{3}a_0 \times 45c_0$ for 20 keV events, where a_0 and c_0 are the HCP lattice parameters. They contained 250 880 and 532 360 atoms, respectively. In order to generate meaningful statistics, eight cascades were simulated for each metal at each PKA energy.

Each perfect-crystal block was equilibrated for at least 10 ps at 100 K before the primary recoil was initiated. Although this is a low temperature compared with that experienced by reactor core components, it is the same as that used previously for the MD simulation of HCP metals, as well as several others, and thus offers scope for comparison. The heat imparted to the MD blocks was not extracted and this insulated condition resulted in a rise in temperature of several hundred degrees by the end of a cascade process. However, MD studies for iron and copper where the initial temperature of the block has been varied have indicated that irradiation temperature has only a small effect on the primary cascade damage state [9–11]. The directions used for the PKA were the same high-index crystallographic directions as those chosen for the previous simulations, although it may be noted that no correlation between the final damage state and the PKA direction was found in those studies.

The interatomic potentials employed were many-body functions of the Finnis–Sinclair type and the model crystals exhibit many of the physical properties of the two metals [12]. They have threshold-displacement energies, E_d, that are close to the experimental values. The vacancy formation energy is predicted to be 1.79 eV and 1.59 eV for zirconium and titanium, respectively. Several configurations of self-interstitial atoms (SIAs) are stable in the static lattice, as is generally found for models of the HCP metals [13,14]. The most likely ones are shown schematically in Fig. 1. In the model of zirconium used here, the basal-split (BS) dumbbell has a formation energy of 3.76 eV, followed by the basal crowdion (BC) with 3.77 eV and

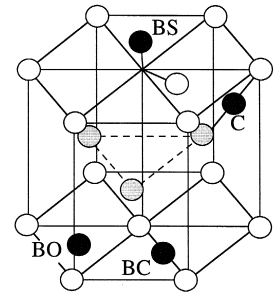

Fig. 1. Four favoured sites for the self-interstitial atom in the zirconium and titanium models used here. They are the basal-split (BS) dumbbell, the basal crowdion (BC), the basal octahedral (BO) and the $\langle 20\bar{2}3 \rangle$ pseudo-crowdion (C).

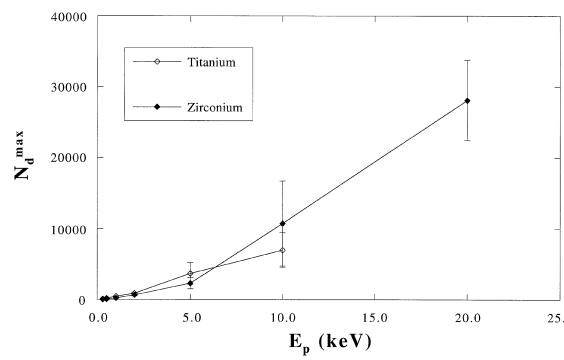

(a)

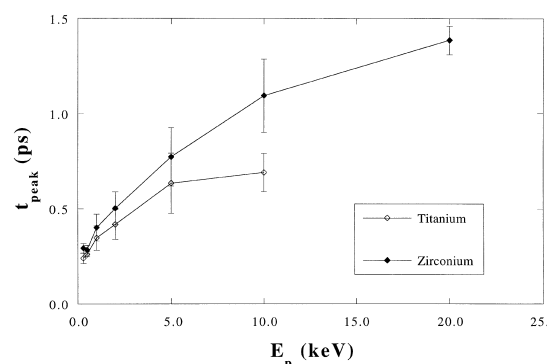

(b)

Fig. 2. Data for both zirconium and titanium showing the variation with PKA energy, E_p, of (a) the maximum number, N_d^{max}, of displaced atoms and (b) the time, t_{peak}, to reach this state. The data points are the means and the bars represent the standard deviations. (The data for $E_p \leq 5$ keV are taken from Refs. [5,6].)

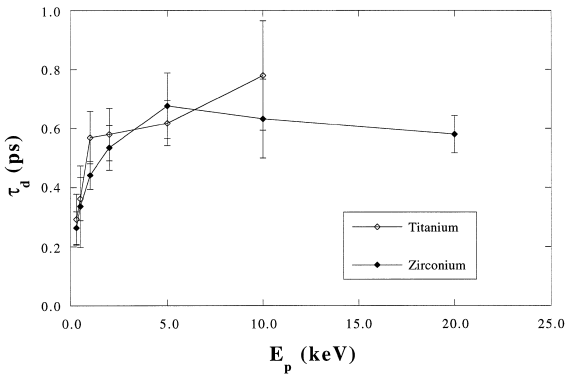

Fig. 3. Data for both zirconium and titanium showing the variation with PKA energy, E_p, of the relaxation time, τ_d, in the number of displaced atoms during the athermal recombination immediately after the time t_{peak}. The data points are the means and the bars represent the standard deviations. (The data for $E_p \leq 5$ keV are taken from Refs. [5,6].)

the basal octahedral (BO) with 3.97 eV. The metastable non-basal SIA at 0 K is the $\langle 20\bar{2}3\rangle$ pseudo-crowdion (C) with an energy of 4.00 eV. The corresponding energies for the SIAs in titanium are 3.07, 3.09, 3.11 and 3.65 eV, respectively.

The similar magnitude of the formation energy of the basal-site interstitials in each metal shows that they undergo thermal migration preferentially in the basal plane, and this has been confirmed explicitly for zirconium by using MD to model the movement of single and multiple interstitial defects [15]. The migration energy for $\langle 11\bar{2}0\rangle$ motion in the basal plane for the SIA is only about 0.01 eV, and that for non-basal motion is an order of magnitude higher. For di- and tri-interstitial clusters, the stable arrangements are near-neighbour defects with their axes aligned along $\langle 11\bar{2}0\rangle$ (see Ref. [6]), so that they form small interstitial dislocation-like loops with Burgers vector $\boldsymbol{b} = 1/3\langle 11\bar{2}0\rangle$, as first described by Bacon [13]. By use of computer visualisation, these clusters are found to move easily by thermal migration along their glide prism in the basal plane with an activation energy of about 0.01 eV [15].

3. Ballistic and relaxation phases of cascade formation

During the ballistic phase of a cascade, the PKA sets up a avalanche of atomic collisions, the total kinetic energy of the atoms reaches a minimum and the potential energy a maximum. It is characterised by a rapid increase in the number of atoms displaced from their lattice sites as the shock wave from the 'explosive' cascade core moves outwards. In the previous studies, this phenomenon was visualised by use of computer-generated plots showing displaced atoms at different times (see figs. 2 and 3 of Ref. [5], for example). Such atoms were defined by the criterion that they do not lie within $0.32\,a_0$ of an atomic site of the perfect crystal. An atom displaced in this way before this final state is reached does not necessarily represent a *stable* interstitial defect. However, this definition allows SIAs in the cold crystal to be visualised in their appropriate form, e.g., a BS defect is plotted as two interstitial atoms and one vacant site, and a BC defect is seen as three displaced atoms and two vacancies.

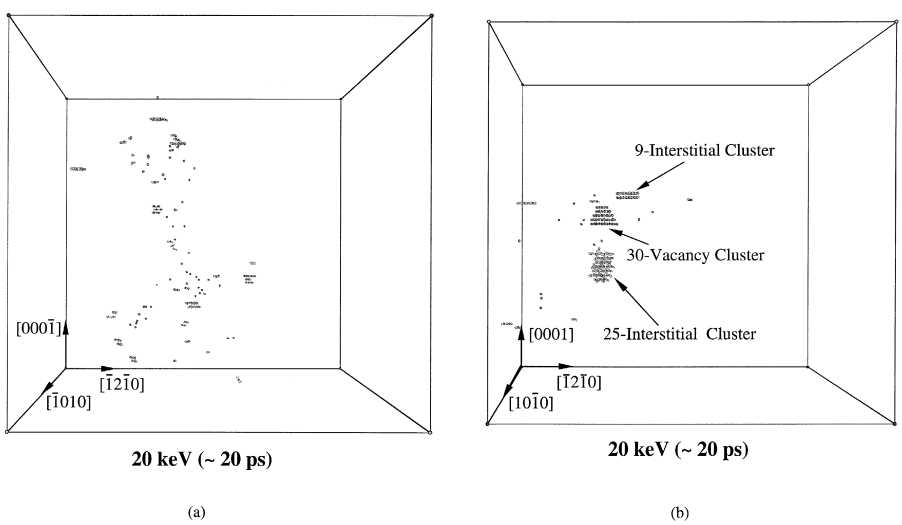

Fig. 4. Computer-generated plots showing the defects created by two different 20 keV cascades in zirconium at 100 K. Displaced atoms (large spheres) are shown as interstitials if they do not lie within $0.32\,a_0$ of a lattice site, and vacancies (small spheres) represent sites where no atom lies within $0.32\,a_0$ of it. The MD box of 531,360 atoms has dimensions of $72\,a_0$ along $[\bar{1}2\bar{1}0]$ and $45c_0$ along [0001]. The final state consists of 48 and 43 Frenkel pairs in (a) and (b), respectively, and corresponds to a time of 20 ps from the initiation of the PKA event.

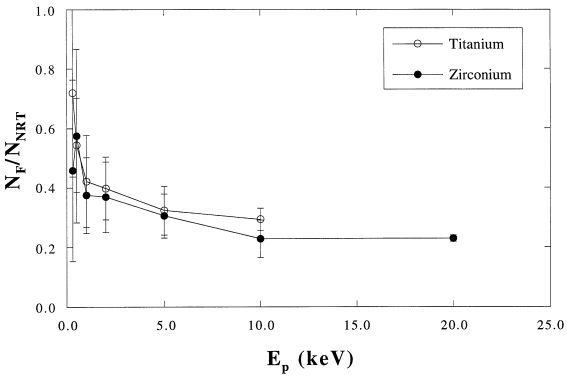

Fig. 5. Variation of the ratio N_F/N_{NRT} with the primary recoil energy E_p in both zirconium and titanium at 100 K. The data points are the mean values over all the cascades at each energy and the bars denote the standard deviation. E_d was taken as 40 eV for zirconium and 30 eV for titanium. (The data for $E_p \leq 5$ keV are taken from Refs. [5,6].)

The extent of the zone of displaced atoms in the ballistic phase is much more extensive for the high-energy cascades in zirconium than that seen previously. This is demonstrated in Fig. 2a and b, where the maximum value, N_d^{max}, of the number of displaced atoms and the time, t_{peak}, at which this maximum is achieved are plotted as functions of E_p for both zirconium and titanium. The values for the lower-energy cascades are included from the earlier work. Each data point represents the mean for all values at that condition and the bars are the standard error. It can be seen that whereas N_d^{max} was smaller for zirconium for E_p up to 5 keV, this is no longer true at higher energy and less than 1.5 eV is required to displace each atom in the high-energy cascades. Also, t_{peak} for zirconium continues to rise over the energy range, in contrast to titanium. It should be noted, however, that there is considerable variability from cascade to cascade. At 20 keV, for example, the extreme values of N_d^{max} were 6275 and 60 525, which gave rise to the minimum and maximum t_{peak} values of 0.82 and 1.62 ps, respectively. The low values of N_d^{max} data correspond to cascades that are diffuse, i.e., the damage zone is spread out, whereas high values occur for cascades where the damage is concentrated in form. Cascades of the latter type tend to result in low levels of defect production in the final cascade state.

A particular feature of the dense, high-energy cascades in zirconium is that although some collision sequences along individual close-packed atomic rows were seen to be emitted from the cascade during the ballistic phase, they occurred early on (after a few tenths of a ps) and were then 'swamped' by the collective, multiple-collision displacements caused by the explosive expansion from the cascade core. Sometimes, the individual sequences resulted in the early creation of SIAs, i.e., they were replacement collision sequences (RCSs), and these defects were found to have survived after the atoms displaced in the period up to t_{peak} had returned to lattice sites.

During the early part of the phase following t_{peak} most of the displaced atoms quickly reoccupy lattice sites, as discussed in [5,6]. This is attributable to the correlated recombination of atoms displaced by short distances from their parent lattice sites in the mantle of radially displaced material surrounding the cascade core. This recombination is athermal in nature and is characterised by the relaxation time τ_d defined by the time $(t_{peak} + \tau_d)$ when the number of displaced atoms, N_d, falls to $1/e$, i.e., 37%, of its maximum N_d^{max}. A plot of $\ln(N_d)$ vs. t is linear with a slope of $(\tau_d)^{-1}$ in the early part of the thermal spike, as found for iron [9] and Ni_3Al [16]. The dependence of τ_d on E_p for both zirconium and titanium is shown in Fig. 3. The data reveal a transition above 2–3 keV at which τ_d becomes constant at about 0.6 ps. A similar dependence of τ_d on E_p was found in iron [9]. It is associated with the changes in cascade morphology which accompany an increase in PKA energy, for as E_p increases, an increasing proportion of displaced atoms is contained in the mantle of collective, focused collision sequences surrounding the hot, highly disordered core.

4. The final defect state

The defects in the final state of the 20 keV cascades in zirconium that were referred to above as having the lowest (6275) and highest (60,525) values of N_d^{max} are shown in Fig. 4a and b, respectively. The vacant sites are represented by small circles and the displaced atoms that constitute SIAs are shown as large circles. Despite the large differences in N_d^{max} and defect arrangement between these two cascades, the difference between the number, N_F, of

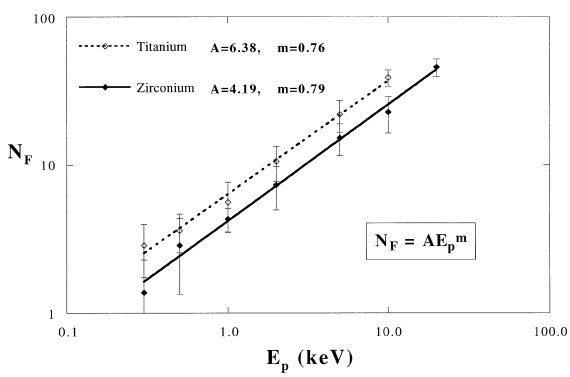

Fig. 6. Variation of N_F with E_p in both zirconium and titanium at 100 K using logarithmic scales to demonstrate the power-law relationship inset in the figure. The data points are the mean values over all the cascades at each energy and the bars denote the standard deviation.

Frenkel pairs is small, viz. 48 and 43 respectively. This difference is discussed in Section 7. The defects in the crystal in Fig. 4a are largely in the form of single point-defects and small clusters, whereas the majority of those in Fig. 4b have formed sizeable clusters, as indicated.

It is well-known from previous studies that N_F increases with increasing E_p, but at a decreasing rate, so that the 'efficiency' of defect production by the cascade process decreases as the cascade energy increases (for reviews see Refs. [1,2]). The number of defects generated per cascade is conventionally estimated by the modified Kinchin and Pease (or NRT) formula [17]:

$$N_{NRT} = 0.8\,E_{dam}/2\overline{E}_d, \quad (1)$$

where E_{dam} is the PKA energy available for displacement damage by elastic collisions (and approximately equals E_p for the energies considered here), $\overline{E}_d$ is the mean value of the displacement threshold energy in the crystal, and 0.8 is an efficiency factor to allow for the fact that atoms in a real crystal do not interact via a simple hard-sphere poten-

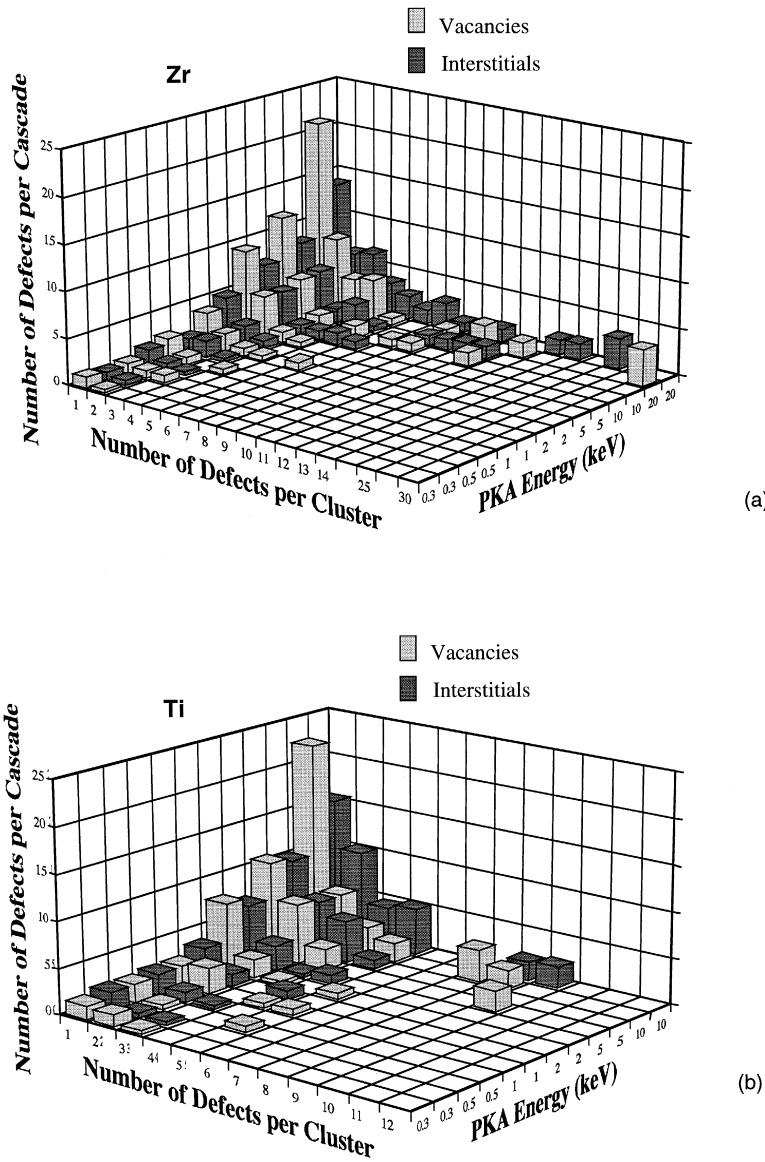

Fig. 7. Data for the number of SIAs in interstitial clusters, and vacancies in vacancy clusters, per cascade as a function of cascade energy in (a) zirconium and (b) titanium at 100 K. Note the discontinuities in the cluster-size scale in (a). The data were obtained by averaging over all cascades at each energy.

tial. The earlier work referred to has shown that cascades produce much lower values of N_F for E_p values above about 1 keV than are predicted by Eq. (1). To show this here, we plot the values of N_F normalised with respect to N_{NRT} for the present simulations and the previous ones on zirconium and titanium in Fig. 5. $\bar{E}_d$ in Eq. (1) was chosen to be 40 eV for zirconium and 30 eV for titanium; these values are those specified in the NRT standard (Standard E521-89, Annual Book of ASTM Standards, ASTM, Philadelphia) and are close to the spatial means in the MD models [12,18]. The two HCP metals behave in a similar fashion to that reported for metals of other crystal structures. The production efficiency (relative to the NRT estimate) in zirconium saturates at about 23% over the energy range 10–20 keV.

Bacon et al. [4] and Wooding et al. [5] have shown that for all the metals simulated to date, N_F has a power-law dependence on E_p (in keV) given by

$$N_F = A(E_p)^m, \quad (2)$$

where A and m lie in the ranges 4.5–6 and 0.7–0.8, respectively. The value of m less than 1 reflects the decreasing efficiency of Frenkel pair production as E_p increases. The new data obtained here fit this relationship well, as shown by the logarithmic plots in Fig. 6. The best-fit values of A and m are 4.195 keV^{-m} and 0.785 for zirconium and 6.38 keV^{-m} and 0.763 for titanium. The higher production efficiency in titanium arises from the larger value of A and may be due to the smaller value of E_d or the reduced intensity of the thermal spike in the lighter metal.

5. Defect clustering

The tendency of defects to cluster in cascades affects their behaviour and influences subsequent changes in microstructure (for example, Refs. [19–21]). MD simulations of several metals have shown that a significant part of the interstitial population is produced in clusters, but that the size of this fraction is dependent on the metal and cascade energy [2]. Some clusters are created by chance at the periphery of the cascade core before the end of the thermal spike, whereas others form by short-range diffusion in the first few ps after this stage. Clustering by the latter process is driven by the large elastic interaction among neighbouring interstitials and small interstitial clusters.

The probability of forming a large cluster increases with increasing PKA energy, as shown by the histogram of cluster-size data for SIAs in zirconium in Fig. 7a. (Note that the scale for the cluster size is not continuous.) The largest SIA cluster found among all the cascades considered contained 25 interstitial atoms and is labelled as such in Fig. 4b. The same cascade also contains a nine-interstitial cluster. The largest cluster in the more-dispersed arrangement in Fig. 4a contains only six interstitials, but it is clear from the histogram that large clusters are not uncommon in zirconium. We shall return to the geometrical nature of these defects in Section 6.

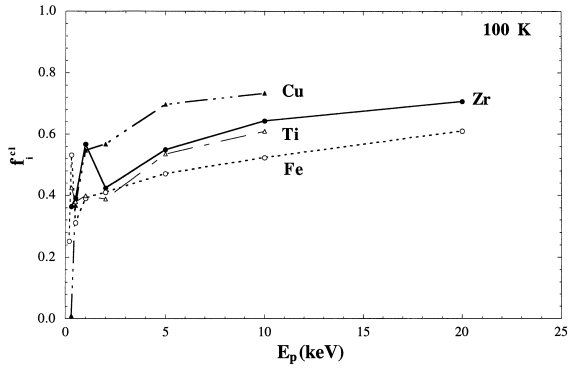

Fig. 8. Variation of the interstitial clustering fraction as a function of cascade energy for cascades in zirconium, titanium, α-iron and copper. The data for the latter two metals are from Refs. [10,22].

The SIA cluster size data for E_p up to 10 keV in titanium are presented in Fig. 7b, from which it may be noted that large clusters are less frequent in this metal. Thus, although N_F is higher in titanium than zirconium (Fig. 6), the fraction of SIAs produced in clusters is actually lower. Fig. 8 shows the fraction, f_i^{cl}, of surviving interstitials that exist in clusters of size two or larger in the two metals. It can be seen that the clustering fraction increases slowly with increasing energy in zirconium and titanium. The f_i^{cl} data for α-iron and copper taken from [10,22] are included for comparison, from which we infer that both titanium and zirconium are intermediate between iron and copper in their clustering fraction.

The cluster data for vacancies are included in Fig. 7a and b. It can be seen that the number of single vacancies is greater than that of single SIAs at energies above about 5 keV, and so the fraction in clusters is less than that for interstitials. Nevertheless, the largest cluster encountered in zirconium is the 30-vacancy defect identified in the cascade in Fig. 4b and the histogram shows that, in comparison with the sizes found in the lower energy cascades [6], vacancy clusters of quite large size can occur in this metal. As in the SIA population, the vacancy clusters in titanium are smaller than those produced at the same energy in zirconium for high E_p.

6. Nature of the large defect clusters

6.1. Interstitial clusters

The most common single SIAs found in cascade debris in both zirconium and titanium at the end of the thermal spike are the stable but degenerate BC and BS defects (see next paragraph). The metastable BO and C forms are

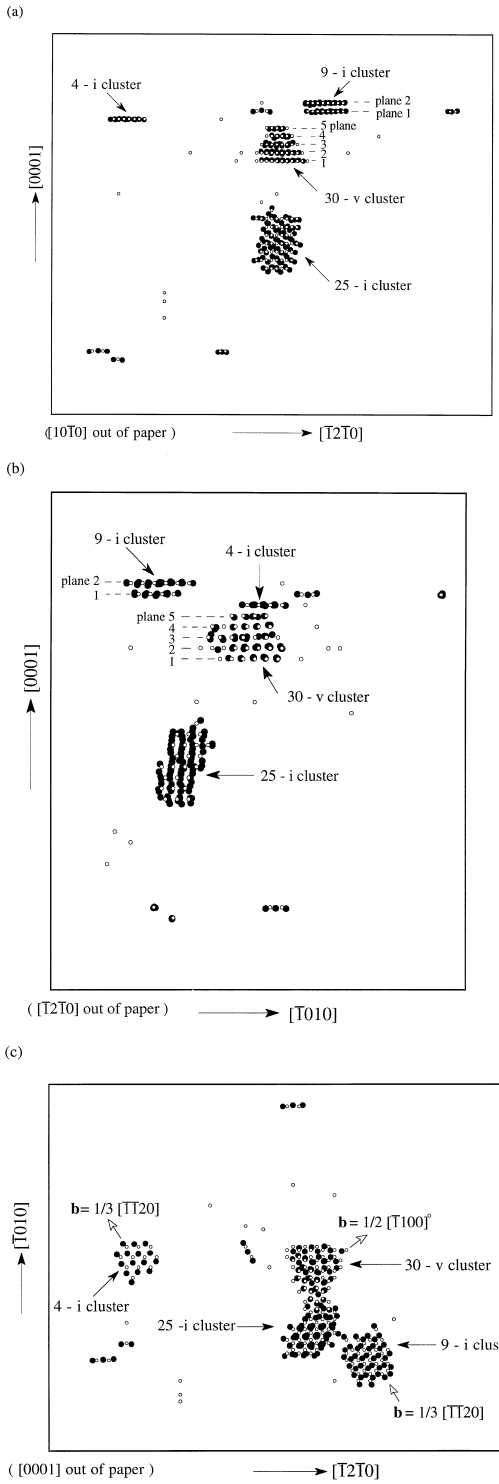

Fig. 9. Orthogonal projections of the vacant sites and atoms in interstitial positions in the 20 keV cascade in zirconium shown on Fig. 4b. The identity of some clusters, their Burgers vector and the planes for which atomic projections are presented in Fig. 10, Fig. 11 and Fig. 13 are as indicated.

observed occasionally. Small clusters of interstitials in their stable state usually adopt a dislocation loop geometry consisting of parallel BC/BS defects. Enlarged visualisations of di-, tri- and tetra-interstitial clusters having this form were shown in fig. 9 of Ref. [6]. Such defects can be described as small dislocation loops with Burgers vector $\boldsymbol{b} = 1/3\langle 11\bar{2}0\rangle$ along the BC/BS axis, as first discussed by Bacon [13]. In visualisations of their behaviour in MD simulations, they are seen to glide back and forth by one-dimensional migration along the direction of **b**. Their mobility is high and comparable with that of the single interstitial [15].

It is of interest to now consider the nature of the much larger clusters created in the high-energy cascades in the present work. Most have the dislocation form of their smaller cousins. As an example, we consider the nine-interstitial defect indicated in Fig. 4b. Parts of the MD box containing this cascade are plotted without perspective in three orthogonal projections in Fig. 9. At this level of scale, the single SIAs are seen to be of either the BS or the BC form (with either two or three displaced atoms, respectively). The SIAs in the four-interstitial cluster all reside in

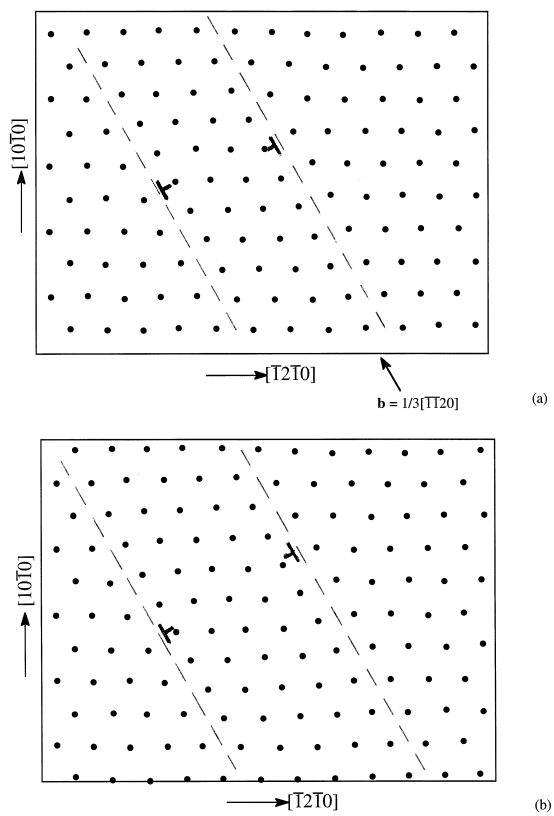

Fig. 10. [0001] projections of the atomic positions in planes 1 and 2 near the nine-interstitial cluster shown in Fig. 4b and Fig. 9. The dashed lines sketched on the figures reveal the dislocation character of this defect.

the same basal plane and those in the nine-interstitial cluster are arranged as four in one plane and five in the plane above. The atomic positions around the latter cluster in these two planes (labelled planes 1 and 2 in Fig. 9a) are plotted in Fig. 10a and b, respectively. From the distortion of the close-packed directions in these planes, it is seen that the cluster has dislocation character with Burgers vector $1/3[\bar{1}\bar{1}20]$ and a glide prism indicated by the dashed lines. The centre of the core can be determined from the location at which the displacement difference between atoms across the glide plane is $b/2$, and this is indicated by the usual dislocation symbol.

The atomic arrangement associated with the large 25-interstitial cluster shown in Fig. 4b and Fig. 9 does not have a simple interpretation. It consists of SIAs occupying sites in eight adjacent basal planes, but plots of atomic positions in sections taken through the cluster in several projection directions do not reveal a structure characteristic of dislocations expected in the HCP lattice. This defect is believed to be a metastable cluster that has not achieved the stable (dislocation) state over the time of the MD simulation ($\sim$ 110 ps).

Another, simpler form of metastable interstitial cluster was found in some cascades in both metals. One variant is a tetra-interstitial and consists of several SIAs arranged in one basal plane such that they adopt a symmetric, equilateral triangle arrangement with ten displaced atoms in a close-packed formation occupying six lattice sites also in a

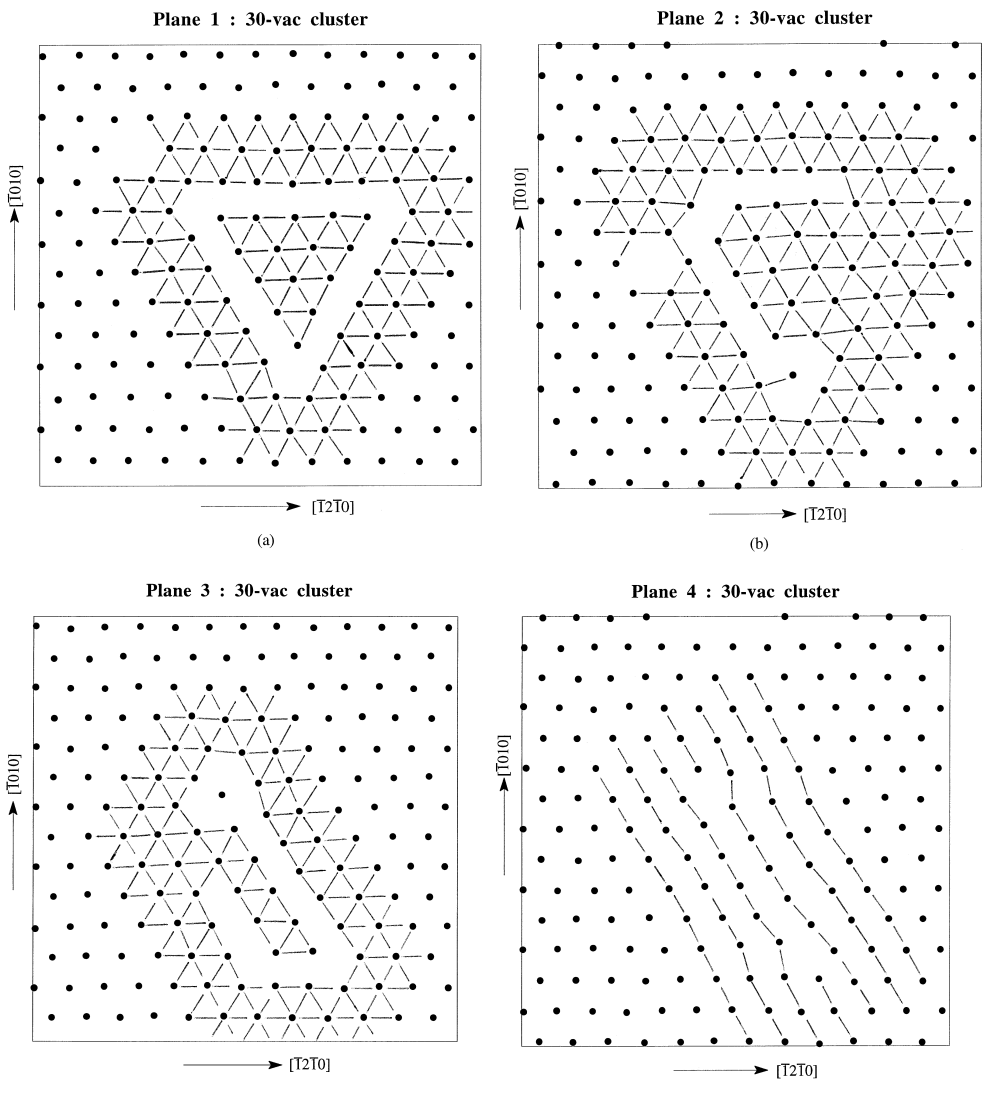

Fig. 11. [0001] projections of the atomic positions in planes 1 to 4 near the 30-vacancy cluster shown in Fig. 4b and Fig. 9. The near-neighbor bonds sketched on the figures reveal the regions where the disregistry in the atomic coordination is strongest.

close-packed triangle. A larger, penta-interstitial variant formed by 15 atoms sharing ten sites was also found in the present work in a 10 keV cascade in zirconium. These triangular defects were produced in two of the 56 cascades created in the present work, and in each case was formed by a defocused event in the ballistic phase that survived subsequent envelopment in the ballistic mantle. They were not observed to migrate during subsequent annealing.

6.2. Vacancy clusters

The data for vacancy agglomerates in Fig. 7 show that they are comparable in size with the interstitial clusters, but analysis of their atomic arrangement reveals that very few can be identified as dislocation-type defects, i.e., they do not readily form the vacancy loops associated with cascade collapse [23]. We would expect the lattice around the largest clusters to have the greatest chance of collapsing to a dislocation configuration, and it is instructive, therefore, to consider the nature of the 30-vacancy cluster identified in the 20 keV cascade in Fig. 4b. As can be seen in more detail in Fig. 9, the vacancies of this defect occupy sites in five adjacent basal planes, but not in a predominant planar fashion expected of a dislocation loop.

The atomic positions on the four basal planes numbered 1–4 in Fig. 9 are plotted in [0001] projection in Fig. 11a–d. Some near-neighbour bonds have been sketched to attempt to provide an interpretation of the structure. In plane 1 (Fig. 11a), it would seem that 15 atoms in a close-packed triangle symmetrically occupy the sites of 21 atoms, i.e., the defect content of six vacancies has been uniformly spread over a triangle with the 15 atoms in a C position in the ABAB... stacking sequence. This is a two-dimensional equivalent of a stacking fault tetrahedron in the FCC metals, which is formally a tetrahedron of atoms centred on a larger tetrahedron hole. A single vacancy also exists away from the triangular defect in this plane. Plane 2 (Fig. 11b), which also contains a single vacancy, has most of its vacancies in a near-triangular arrangement, but now the vacancy content (seven vacancies) is spread around two sides of the triangle. The defect content in plane 3 (Fig. 11c) is again seven vacancies, and in this case the atoms have adopted a line arrangement parallel to the $(1\bar{1}00)$ plane. Finally, the six vacancies in plane 4 (Fig. 11d) have created a structure consistent with removal of part of a $(1\bar{1}00)$ plane and collapse of the surrounding atoms into the hole. The projection has the standard vacancy dislocation-loop form, and although a partial Burgers vector $\boldsymbol{b} = 1/2[\bar{1}100]$ is indicated, it can be seen that atoms immediately adjacent to the loop plane have started to shear to remove the stacking fault formed by the vacancies.

We conclude, therefore, that the vacancy cluster has a three-dimensional, hybrid form consisting of a conventional prism–plane dislocation loop in its upper portion and a (0001) stacking-fault at the bottom. The effect of annealing on this unusual configuration will be discussed in Section 7.

7. Discussion

By combining the new results for the cascades generated in the present work with the low-energy data obtained in the earlier studies of zirconium and titanium, we have been able to assess the effects of cascade energy on defect formation in the two HCP metals over a wide range of PKA energy. Since the atomic collisions in the MD model employed are purely elastic, electronic-energy losses, which are important in real metals for high PKA energy, have been neglected. For this reason, the E_p values quoted are reasonable approximations to the damage energy used in the theory of radiation effects. The other approximation used here was the neglect of accelerated cascade cooling due to coupling of the lattice phonons to the electron system. This process was deliberately ignored because no satisfactory way has been found of incorporating it into MD simulations. Approximate treatments involving damping of hot atoms suggest that it is a second-order effect and likely to result in a slight increase in N_F and may marginally restrict the clustering of defects during the thermal spike.

It was seen in Section 3 that the ballistic phase for 10 and 20 keV cascades in zirconium is long and can exceed 1 ps in time. For 20 keV cascades which have a compact morphology, more than 30 000 atoms are displaced by distances exceeding $0.32\,a_0$, and the resulting thermal spike phase is efficient at effecting recombination of interstitials and vacancies. As a consequence, the final number of Frenkel defects produced by such events is small and typically only about 40, compared with about 50 for the less compact cascades. Similar trends were found for the 10 keV cascades in zirconium, for the extremes of N_d^{max} were 3461 and 18 151 and these two cascades produced the largest (32) and smallest (15) values of N_F, respectively. This demonstrates a general conclusion of this study that cascades that spread out in the ballistic phase generate more vacancies and interstitials overall, whereas those that form a dense core of displacements with no tendency towards subcascade formation create fewer.

It is of possible importance to note that, despite the variability in cascade form and defect production, the power-law dependence of the mean value N_F on E_p (Eq. (2)), first found empirically by Bacon et al. [2] from data for cascades of lower energy, holds for E_p up to 20 keV. As a result, N_F in zirconium is less than 25% of the NRT estimate over the energy range 10–20 keV, and only slightly higher at about 30% in titanium at 10 keV. In the present state of knowledge, it is not possible to state what proportion of the N_F interstitials actually leave a cascade region to become freely migrating defects. That will depend on the extent to which SIA-vacancy recombination

and entrapment of migrating interstitial clusters actually occur within the cascade region itself, and the timescale of this is beyond simulations carried out by MD. However, the fact that N_F is only about 25% of N_{NRT} and the clustering fraction of SIAs is large (Fig. 8) suggests that the freely migrating defects are less than 10% of the NRT value in zirconium.

The cluster data described in Section 5 show that the size and lifetime of the hot disordered core of a cascade also influence the probability of cluster formation in the cascade process itself. Dense, compact cascades produce a higher proportion of the SIA clusters, presumably because of the increased probability of displaced atoms being in close proximity to each other and having more favourable conditions to move and cluster during the thermal spike. The larger vacancy clusters were also created in the cascades with the higher N_d^{max} values. Again, it is not clear if this is simply due to the increased probability of vacancies being in near-neighbour sites or to thermal conditions that sweep vacancies into clusters before final recrystallisation.

The formation of vacancy dislocation-loops and tetrahedra by cascade collapse in ion-irradiated foils is well-known (e.g., Ref. [23]), but the evidence for interstitial-cluster formation during the lifetime of a cascade is less firm. Diffuse X-ray scattering in copper irradiated with neutrons at 4.6 K indicates that they do form [24] and previous MD simulations have revealed small clusters (e.g., Ref. [2]). Stoller [25] found that SIA clusters up to 14 in size are created in MD simulations of cascades of up to 40 keV in energy in α-iron, and the data generated in the present work support the view that interstitial clustering is a key feature of the cascade process.

Interestingly, the cluster size data for both metals in Fig. 7 show that the size of interstitial clusters is on a par with that of the vacancy defects. Since we have already noted that the movement of small interstitial clusters in zirconium and titanium is largely restricted to $\langle 11\bar{2}0\rangle$ paths in the basal plane, it is clear that the large clusters found in the present work were formed during the cascade process without extensive SIA migration. Most of the interstitial clusters are glissile loops with perfect $1/3\langle 11\bar{2}0\rangle$-type Burgers vectors. They were observed in computer visualisations to be mobile and it is anticipated that their preference for basal-plane motion will affect the evolution of the radiation damage microstructure in zirconium.

As noted in Section 6.1, a triangular array of interstitial atoms in the basal plane was created during the cascade process itself in two of the current simulations. An extended defect of this type was first seen with static simulations using pair potentials [13], and was a tri-interstitial consisting of six atoms symmetrically arranged around three lattice sites (see fig. 10b of Ref. [13]). It was found to be metastable with respect to a $1/3\langle 11\bar{2}0\rangle$ tri-interstitial loop and to exist as a triangle of atoms in C positions in one atomic plane of the normal HCP stacking sequence ABABAB.... The fact that the tetra- and penta-interstitial variants – with ten atoms sharing six sites and 15 atoms sharing ten sites, respectively – were generated dynamically in the present work suggests that the formation of such metastable defects may not be uncommon in zirconium and titanium. Their strain field is largely confined to their basal plane and they would not be readily detectable. Their lifetime before transforming to a stable dislocation state (such as that of the tetra-interstitial projected in Fig. 9c) would depend on the temperature or on the probability of capture of another SIA, which would destroy the triangular arrangement.

The other metastable interstitial cluster found here was the 25-SIA defect shown in Fig. 4b and Fig. 9. To study the possible change in this and the other defects during the immediate aftermath of the thermal spike, the two 20 keV cascades presented in Fig. 4a and b were annealed by continuing the simulations for over 100 ps. Over this post-cascade period, the average temperature in the MD cell was between 200 and 300 K. The defect debris at this time is plotted in Fig. 12. By comparing the arrangement of damage in this figure with that in Fig. 4, it can be seen that the vacancies have not moved over this time, but that considerable motion of the small clusters of interstitials has occurred. However, the large, 25-SIA defect did not reorganise its atomic structure to establish an identifiable dislocation character. It is of interest to note that Stoller [22] observed the creation of metastable clusters of interstitials in MD simulations of high-energy cascades in α-iron, and it therefore seems probable that metastable arrangements can exist for a considerable time after the cascade event in irradiated metals.

In terms of the effect of short-term annealing on defect numbers, the cascade in Fig. 4b and Fig. 12b, initially had five single SIAs and two joined to form a di-interstitial, but N_F did not change. The cascade in Fig. 4a has 29 single vacancies and 16 single SIAs, and after 110 ps, two SIAs recombined with vacant sites, reducing N_F from 48 to 46, and three SIAs clustered to increase the number of tri-interstitials from four to five and reduce the number of single interstitials to eleven. Thus, it may be concluded that the defect structure of the more diffuse cascades is more strongly affected by post-cascade annealing than that of the more-strongly-clustered dense cascades.

Although vacancies and their small clusters did not migrate during the anneal to 110 ps, some rearrangement of the atoms around the 30-vacancy defect in the cascade in Fig. 4b and Fig. 12b did occur. This is illustrated by the [0001] projections of atoms in Fig. 13a and b: they correspond to the projections in Fig. 11a and b, and are the planes labelled 1 and 2 in Fig. 9. (The atomic positions in Fig. 11c and d for the planes labelled 3 and 4 hardly change during the anneal.) By sketching in some near-neighbour bonds to emphasize where the atomic disregistry is greatest and comparing Fig. 13 with Fig. 11, it can be seen that the HCP atomic coordination has been more

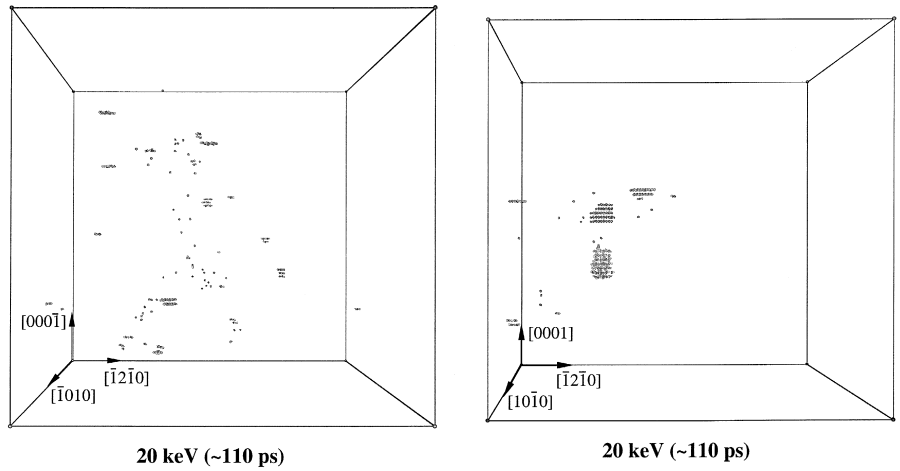

Fig. 12. Defect plots for the two 20 keV cascades in zirconium shown in Fig. 4 after annealing for a further 90 ps.

clearly established on the right of the two triangular regions identified in Fig. 11a and b. Thus, over the time of the additional simulation, the cluster has changed to become a more-clearly defined faulted loop in the $(1\bar{1}00)$ prism plane with a $1/2[\bar{1}100]$ Burgers vector. The key point is that cascade collapse to a dislocation loop is not complete by the end of the thermal spike but occurs over a timescale of the order of 100 ps.

At this point, it is appropriate to summarise current knowledge of cascade damage in the HCP metals, based on theoretical and experimental work. In order to investigate the mechanism of vacancy-loop nucleation in the depleted zones of displacement cascades in zirconium, Kapinos et al. [26] used molecular dynamics with a non-equilibrium pair potential to study the behaviour of vacancy-rich zones in the presence of a thermal spike. The type of vacancy loop nucleated (i.e., basal or prism orientation) was found to depend on the average volume concentration of vacancies, C_v, in the depleted zone at the moment of its crystallization during cooling. For $C_v = 10\%$

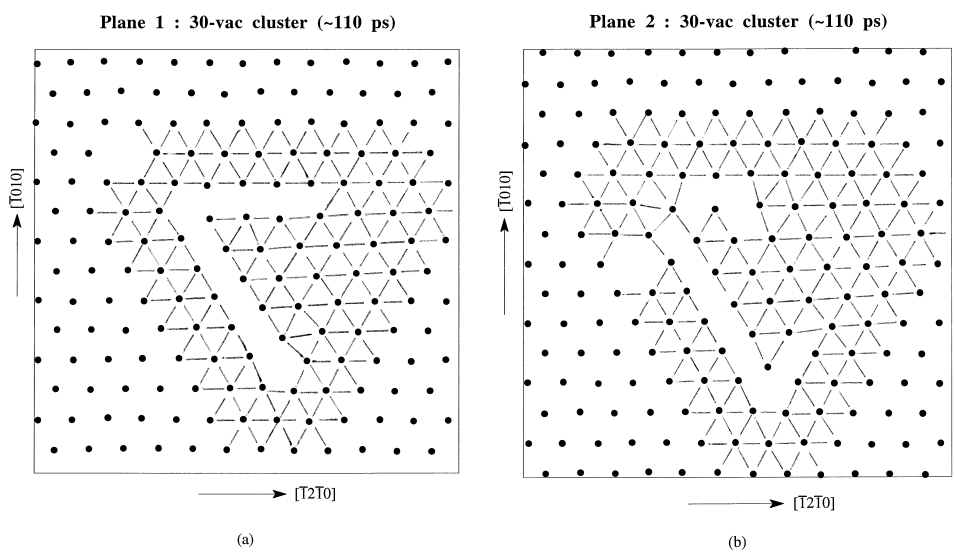

Fig. 13. [0001] projections of the atomic positions in planes 1 and 2 near the 30-vacancy cluster after 110 ps (Fig. 12b). The near-neighbor bonds sketched on the figures reveal the regions where the disregistry in the atomic coordination is strongest.

the nucleation of $\{10\bar{1}0\}$ prism–plane vacancy dislocation loops with Burgers vector $\boldsymbol{b} = 1/2\langle 10\bar{1}0\rangle$ and $1/3\langle 11\bar{2}0\rangle$ was observed. For $C_v = 15\%$, basal-plane loops with $\boldsymbol{b} = 1/6\langle 20\bar{2}3\rangle$ were nucleated. These observations raise an interesting point as to whether a similar tendency would have been found in the present work if an appreciably larger number of PKA events had been simulated.

Previous experimental investigations of cascade damage have included the direct observation in a transmission-electron-microscope (TEM) of small defects exhibiting the strain-contrast features of dislocation loops produced in collision cascades. The earliest used oxide-coated emission filaments to provide a beam consisting of heavy ions and electrons, thus providing simultaneous 100 keV ion bombardment (at 20 K) and TEM observation. For HCP cobalt ($c/a = 1.62$), Howe and Rainville [27] found the defect yield (= number of visible dislocation loops per unit area/number of incident ions per unit area) to be 0.06, with the majority of loops having diameters of 1.5 to 4.0 nm. They were vacancy in character with strain fields consistent with that expected for loops lying on the (0001) plane with $\boldsymbol{b} = 1/6\langle 20\bar{2}3\rangle$. In zirconium [28], the yield of loops was also low (~ 0.05) and the majority again had diameters of 1.5 to 4.0 nm. A yield of ~ 0.15 was observed for loops in zirconium irradiated with 30 keV Bi ions at 35 K and subsequently examined by TEM at 295 K [29]. Föll and Wilkens [30] also found that vacancy loops (of 3 to 13 nm diameter) were produced in HCP cobalt during bombardment at 295 K with 60 keV Au ions to fluences of 10^{15} to 5×10^{16} ions m^{-2}. They concluded that most of the loops were on $\{10\bar{1}0\}$ planes with $\boldsymbol{b} = 1/3\langle 11\bar{2}0\rangle$ but that a small fraction consisted of pure-edge, faulted loops with $\boldsymbol{b} = 1/2\langle 10\bar{1}0\rangle$. The defect yield and cascade efficiency (= number of vacancies in the visible loops/theoretical number of vacancies initially produced in the collision cascades according to the NRT estimate) were 0.07 and 0.56, respectively.

More recently, detailed TEM studies have been performed on HCP ruthenium ($c/a = 1.58$) and titanium ($c/a = 1.59$) following bombardment at ~ 295 K with heavy ions to fluencies of 2×10^{15} to 5×10^{15} ions m^{-2}. The irradiations were performed with a range of ion mass (from ^{84}Kr to ^{184}W) and ion energies from 30 to 100 keV. In ruthenium [31–33], it was found that in the majority of the cases displacement-cascade collapse resulted in the formation of small faulted vacancy-loops (1.7 to 2.4 nm average diameter) on the $\{10\bar{1}0\}$ prism planes with $\boldsymbol{b} = 1/2\langle 10\bar{1}0\rangle$. Some of these subsequently unfaulted to form perfect $1/3\langle 11\bar{2}0\rangle$ loops. The defect yield increased (from ~ 0.15 to ~ 0.4) and the cascade efficiency decreased (from ~ 0.4 to ~ 0.1) with increasing ion energy. Interestingly, the yield increased with increasing ion mass at low energy and decreased at high energy. The latter effect was considered to be due to the formation of sub-cascades by the lighter ions at high energy. In some instances, cascades collapsed on the basal plane to form $1/2[0001]$ loops and some of these transformed to a lower energy configuration with $\boldsymbol{b} = 1/6\langle 20\bar{2}3\rangle$. Basal loops were more common in foils irradiated along a direction lying in the basal plane, suggesting a possible connection between loop crystallography and cascade shape. In titanium foils irradiated with Sb, Sb_2 and Sb_3 ions of energy 50 to 150 keV, it was found that vacancy-loop formation in the centre of the cascades occurred with a very low efficiency for implantation with atomic ions [34,35]. However, implantations with Sb_2 and Sb_3 ions resulted in defect yields of 0.4 to 1 and cascade efficiencies up to 0.4. It was argued that this reflects a considerable sensitivity of vacancy loop formation to the conditions in the cascade core. The defects observed were predominantly either faulted or perfect loops lying on the prism planes.

Turning to experimental results on the development of dislocation loops and dislocation networks in zirconium under conditions where appreciable mobility of interstitials and vacancies is possible, vacancy and interstitial dislocation loops having $\boldsymbol{b} = 1/3\langle 11\bar{2}0\rangle$ coexist during neutron and electron irradiation [36,37]. They are generally aligned in rows or layers parallel to (0001). At temperatures above ~ 723 K, there is a pronounced decrease in the stability of the vacancy loops. Electron irradiation at 573 to 773 K also produces vacancy loops with $\boldsymbol{b} = 1/2[0001]$, interstitial loops with $\boldsymbol{b} = 1/3\langle 11\bar{2}3\rangle$ and loops of undetermined character with $\boldsymbol{b} = 1/6\langle 2023\rangle$. Vacancy loops with $\boldsymbol{b} = 1/6\langle 20\bar{2}3\rangle$ have been observed in zirconium and zirconium alloys with a high interstitial solute content following neutron irradiation at 560 to 773 K. Irradiation damage in the HCP metals such as zirconium, magnesium and titanium appears to be particularly sensitive to impurities and alloying additions [37]. In general, impurities tend to stabilize defects having a [0001] component of $\boldsymbol{b}$.

It is unfortunate that the PKA energy range that can be employed in MD simulations of cascades is below that used to create visible defects in the experiments. However, the MD results presented here are consistent qualitatively with the observations above as both vacancy and interstitial clusters were produced in the cascades and could act as nuclei for dislocation loop formation at higher temperatures. The interstitial clusters were found to be predominantly prism–plane dislocation loops and this is consistent with the experimental findings. Vacancy loops formed by cascade collapse have been found only rarely in MD simulations, probably because the PKA energies considered have been too low, for, as noted above, the experimental loop yield is small even for irradiations with ion energy in the range 30 to 100 keV. A large number of simulations would be required to generate statistics comparable with experiment. However, a large vacancy cluster was created in one of the 20 keV cascades in the present work and transformed over time into a faulted loop on a $\{10\bar{1}0\}$ prism plane with $\boldsymbol{b} = 1/2\langle 10\bar{1}0\rangle$. This is entirely consistent with the experimental observations. The experiments suggest that basal-plane loops only form under

certain conditions, e.g., when either the cascade core has high vacancy and energy densities or solute atoms are present to stabilise vacancy clusters on the basal plane. With the exception of the thermal-spike model in Ref. [26], these conditions have not yet been treated in simulation studies of cascades.

The conclusion from MD that clustering of both SIAs and vacancies takes place in collision cascades in zirconium is also consistent with experimental and computer studies of other metals. As discussed recently in Refs. [20,21], the fact that the proportion of the total defects retained in clusters and their size distributions are different for the primary interstitial and vacancy clusters, and that these differences are temperature-dependent due to different thermal stabilities, should be taken into account in the modelling of radiation-damage effects. The computer simulation method provides a quantitative description of defect number and configuration in the primary damage state. A more detailed treatment of MD simulations for collision cascades in zirconium (including ones at elevated temperatures) is now required to analyse further the evolution of cascade damage and compare it with the experimental data for microstructural evolution and property changes in this metal.

8. Conclusions

(i) Cascades have been simulated with energy, E_p, up to 20 keV in α-zirconium and 10 keV in α-titanium. When combined with the results of previous simulations of cascades of lower energy [5,6], this provides a large data set on cascade damage in these metals.

(ii) Cascades are very variable in form at high energy and this affects the final defect state. Cascades that spread over a larger volume have fewer atoms temporarily displaced in the ballistic phase, have a shorter thermal-spike phase, create more Frenkel pairs and have a lower probability of producing defect clusters.

(iii) The production efficiency of Frenkel pairs in cascades in zirconium falls to about 0.25 of the NRT value as the cascade energy rises above 10 keV. The efficiency is a little higher at about 0.3 of NRT in titanium.

(iv) The power-law dependence of the number of Frenkel pairs, N_F, on E_p found previously:

$$N_F = A(E_p)^m$$

is obeyed by the cascades in the present study.

(iv) Interstitial and vacancy clusters with sizes of the same order are created in the cascade process. Clusters containing up to 25 interstitials and 30 vacancies were formed in zirconium by 20 keV cascades.

(v) Two thirds of the SIAs are produced in clusters in zirconium at high cascade energy. Most clusters have dislocation character with perfect Burgers vectors of the form $1/3\langle 11\bar{2}0\rangle$. A few metastable clusters are formed and are persistent over the timescale of MD simulations.

(vi) Collapse of the 30-vacancy cluster to a faulted loop on the prism plane was found to occur over a period of more than 100 ps.

(vii) Annealing over this timescale has more effect on the number and clustering of defects in cascades that are dispersed over a large region of crystal than in cascades that form a compact region of damage.

(viii) The defect clusters found in the simulations are consistent with dislocation loops observed experimentally in irradiated zirconium.

Acknowledgements

The authors acknowledge the financial support of the CANDU Owners Group (Working Party 32) and the Engineering and Physical Sciences Research Council in carrying out this research.

References

[1] D.J. Bacon, T. Diaz de la Rubia, J. Nucl. Mater. 216 (1994) 275.
[2] D.J. Bacon, A.F. Calder, F. Gao, V.G. Kapinos, S.J. Wooding, Nucl. Instr. Meth. B 102 (1995) 37.
[3] D.J. Bacon, in: H.O. Kirchner, L.P. Kubin, V. Pontikis (Eds.), Computer Simulation in Materials Science, Kluwer Academic, Dortrecht, 1996, p. 189.
[4] D.J. Bacon, A.F. Calder, F. Gao, Rad. Eff. Def. Sol. 141 (1997) 283.
[5] S.J. Wooding, D.J. Bacon, W.J. Phythian, Philos. Mag. A 72 (1995) 1261.
[6] S.J. Wooding, D.J. Bacon, Philos. Mag. A 76 (1997) 1033.
[7] V. Fidleris, J. Nucl. Mater. 159 (1988) 22.
[8] C. Lemaignan, A.T. Motta, Nuclear Materials, in: B.R.T. Frost (Ed.), Vol. 10B of Materials Science and Technology; a Comprehensive Treatment, VCH, Weinheim, 1994, p. 1.
[9] A.F. Calder, D.J. Bacon, J. Nucl. Mater. 207 (1993) 25.
[10] W.J. Phythian, R.E. Stoller, A.J.E. Foreman, A.F. Calder, D.J. Bacon, J. Nucl. Mater. 223 (1995) 245.
[11] F. Gao, D.J. Bacon, P.E.J. Flewitt, T.A. Lewis, J. Nucl. Mater. 249 (1997) 77.
[12] G.J. Ackland, S.J. Wooding, D.J. Bacon, Philos. Mag. A 71 (1995) 553.
[13] D.J. Bacon, J. Nucl. Mater. 159 (1988) 176.
[14] D.J. Bacon, J. Nucl. Mater. 206 (1993) 249.
[15] B. Whiting, D.J. Bacon, Microstructure evolution during irradiation, in: I.M. Robertson, G.S. Was, L.W. Hobbs and T. de la Rubia (Eds.), Sympos. Proc., Vol. 439, Materials Research Society, Pittsburgh, 1997, p. 389.
[16] F. Gao, D.J. Bacon, Philos. Mag. A 71 (1995) 43.
[17] L.K. Norgett, M.T. Robinson, I.M. Torrens, Nucl. Eng. Design 33 (1975) 50.
[18] S.J. Wooding, D.J. Bacon, Rad. Eff. Def. Sol. 130&131 (1994) 461.

[19] C.H. Woo, B.N. Singh, Philos. Mag. A 65 (1992) 889.
[20] C.H. Woo, A.A. Semenov, B.N. Singh, J. Nucl. Mater. 206 (1993) 170.
[21] B.N. Singh, J.H. Evans, J. Nucl. Mater. 226 (1995) 277.
[22] R.E. Stoller, Microstructure of irradiated materials, in: I.M. Robertson, L.E. Rehn, S.J. Zinkle, W.J. Phythian (Eds.), Sympos. Proc., Vol. 373, Materials Research Society, Pittsburgh, 1995, p. 21.
[23] C.A. English, M.L. Jenkins, Mater. Sci. Forum 15–18 (1987) 1003.
[24] R. Rauch, J. Peisl, A. Schmalzbauer, G. Wallner, J. Nucl. Mater. 168 (1989) 101.
[25] R.E. Stoller, private communication.
[26] V.G. Kapinos, Y.N. Osetsky, P.A. Platonov, Mater. Sci. Forum 97–99 (1992) 235.
[27] L.M. Howe, M.H. Rainville, Phys. Status Solidi A 7 (1971) 125.
[28] L.M. Howe, unpublished results (1967).
[29] L.M. Howe, unpublished results (1991).
[30] H. Föll, M. Wilkens, Phys. Status Solidi 39 (1977) 561.
[31] W.J. Phythian, B.L. Eyre, D.J. Bacon, C.A. English, Philos. Mag. A 55 (1987) 757.
[32] W.J. Phythian, J. Nucl. Mater. 159 (1988) 219.
[33] W.J. Phythian, C.A. English, D.J. Bacon, B.L. Eyre, Philos. Mag. A 62 (1990) 617.
[34] D.H. Yellen, D.J. Bacon, W.J. Phythian, C.A. English, Vacuum 39 (1989) 1141.
[35] D.H. Yellen, D.J. Bacon, W.J. Phythian, C.A. English, Proc. 15th Symp. on Effects of Radiation on Materials, Nashville, TN, June 1990, ASTM-STP 1125, 1992, p. 385.
[36] M. Griffiths, J. Nucl. Mater. 159 (1988) 190.
[37] M. Griffiths, Philos. Mag. A 63 (1991) 835.